



Spatial and temporal identification of cerebral infarctions based on multiphoton microscopic imaging

SHU WANG,^{1,5} HUIPING DU,^{1,5} BINGBIN LIN,^{2,5} CHENXI LIAO,¹ XIAOQIN ZHU,^{1,6} XINGFU WANG,³ HONG CHEN,³ SHUANGMU ZHUO,¹ LIWEI JIANG,¹ LIANHUANG LI,¹ HAOHUA TU,⁴ AND JIANXIN CHEN^{1,7}

¹Key Laboratory of OptoElectronic Science and Technology for Medicine of Ministry of Education, Fujian Provincial Key Laboratory of Photonics Technology, Fujian Normal University, Fuzhou 350007, China

²Fujian University of Traditional Chinese Medicine, Fuzhou 350122, China

³Department of Pathology, The First Affiliated Hospital, Fujian Medical University, Fuzhou 350001, China

⁴Beckman Institute for Advanced Science and Technology, University of Illinois at Urbana-Champaign, Urbana, IL 61801, USA

⁵These authors contributed equally to this work.

⁶zhuxq@fjnu.edu.cn

⁷chenjianxin@fjnu.edu.cn

Abstract: Ischemic stroke is a leading cause of death and permanent disability worldwide. Middle cerebral artery occlusion (MCAO) of variable duration times could be anticipated to result in varying degrees of injury that evolve spatially over time. Therefore, investigations following strokes require information concerning the spatiotemporal dimensions of the ischemic core as well as of perilesional areas. In the present study, multiphoton microscopy (MPM) based on two-photon excited fluorescence (TPEF) and second harmonic generation (SHG) was applied to image such pathophysiological events. The ischemic time-points for evaluation were set at 6, 24, 48, and 72 hours after MCAO. Our results demonstrated that MPM has the ability to not only identify the normal and ischemic brain regions, but also reveal morphological changes of the cortex and striatum at various times following permanent MCAO. These findings corresponded well with the hematoxylin and eosin (H&E) stained tissue images. With the technologic progression of miniaturized imaging devices, MPM can be developed into an effective diagnostic and monitoring tool for ischemic stroke.

© 2018 Optical Society of America under the terms of the [OSA Open Access Publishing Agreement](#)

OCIS codes: (180.4315) Nonlinear microscopy; (190.1900) Diagnostic applications of nonlinear optics.

References and links

1. Z. B. Zhou, L. Meng, A. W. Gelb, R. Lee, and W. Q. Huang, "Cerebral ischemia during surgery: an overview," *J. Biomed. Res.* **30**(2), 83–87 (2016).
2. T. Hirano, "Searching for salvageable brain: the detection of ischemic penumbra using various imaging modalities?" *J. Stroke Cerebrovasc. Dis.* **23**(5), 795–798 (2014).
3. P. Lipton, "Ischemic cell death in brain neurons," *Physiol. Rev.* **79**(4), 1431–1568 (1999).
4. T. L. Butler, C. A. Kassed, P. R. Sanberg, A. E. Willing, and K. R. Pennypacker, "Neurodegeneration in the rat hippocampus and striatum after middle cerebral artery occlusion," *Brain Res.* **929**(2), 252–260 (2002).
5. J. Koizumi, Y. Yoshida, T. Nakazawa, and G. Ooneda, "Experimental studies of ischemic brain edema, I: a new experimental model of cerebral embolism in rats in which recirculation can be introduced in the ischemic area," *Jpn. J. Stroke* **8**(1), 1–8 (1986).
6. Y. Liu, G. Tang, Y. Li, Y. Wang, X. Chen, X. Gu, Z. Zhang, Y. Wang, and G. Y. Yang, "Metformin attenuates blood-brain barrier disruption in mice following middle cerebral artery occlusion," *J. Neuroinflammation* **11**(1), 177 (2014).
7. Q. Hu, X. Liang, D. Chen, Y. Chen, D. Doycheva, J. Tang, J. Tang, and J. H. Zhang, "Delayed hyperbaric oxygen therapy promotes neurogenesis through reactive oxygen species/hypoxia-inducible factor-1 α / β -catenin pathway in middle cerebral artery occlusion rats," *Stroke* **45**(6), 1807–1814 (2014).

8. V. Jolivel, F. Bicker, F. Binamé, R. Ploen, S. Keller, R. Gollan, B. Jurek, J. Birkenstock, L. Poisa-Beiro, J. Bruttger, V. Opitz, S. C. Thal, A. Waisman, T. Bäuerle, M. K. Schäfer, F. Zipp, and M. H. H. Schmidt, "Perivascular microglia promote blood vessel disintegration in the ischemic penumbra," *Acta Neuropathol.* **129**(2), 279–295 (2015).
9. A. Popp, N. Jaenisch, O. W. Witte, and C. Frahm, "Identification of ischemic regions in a rat model of stroke," *PLoS One* **4**(3), e4764 (2009).
10. J. Ramos-Cejudo, M. Gutiérrez-Fernández, B. Rodríguez-Frutos, M. Expósito Alcaide, F. Sánchez-Cabo, A. Dopazo, and E. Díez-Tejedor, "Spatial and temporal gene expression differences in core and periinfarct areas in experimental stroke: a microarray analysis," *PLoS One* **7**(12), e52121 (2012).
11. K. Deguchi, N. Liu, W. Liu, Y. Omote, S. Kono, T. Yunoki, S. Deguchi, T. Yamashita, Y. Ikeda, and K. Abe, "Pericyte protection by edaravone after tissue plasminogen activator treatment in rat cerebral ischemia," *J. Neurosci. Res.* **92**(11), 1509–1519 (2014).
12. J. C. Baron, D. Rougemont, F. Soussaline, P. Bustany, C. Crouzel, M. G. Boussier, and D. Comar, "Local interrelationships of cerebral oxygen consumption and glucose utilization in normal subjects and in ischemic stroke patients: a positron tomography study," *J. Cereb. Blood Flow Metab.* **4**(2), 140–149 (1984).
13. C. S. Kidwell, J. R. Alger, and J. L. Saver, "Beyond mismatch: evolving paradigms in imaging the ischemic penumbra with multimodal magnetic resonance imaging," *Stroke* **34**(11), 2729–2735 (2003).
14. M. Wintermark, A. E. Flanders, B. Velthuis, R. Meuli, M. van Leeuwen, D. Goldsher, C. Pineda, J. Serena, I. van der Schaaf, A. Waaijer, J. Anderson, G. Nesbit, I. Gabriely, V. Medina, A. Quiles, S. Pohlman, M. Quist, P. Schnyder, J. Bogousslavsky, W. P. Dillon, and S. Pedraza, "Perfusion-CT assessment of infarct core and penumbra: receiver operating characteristic curve analysis in 130 patients suspected of acute hemispheric stroke," *Stroke* **37**(4), 979–985 (2006).
15. J. G. Merino and S. Warach, "Imaging of acute stroke," *Nat. Rev. Neurol.* **6**(10), 560–571 (2010).
16. Y. Li, C. Powers, N. Jiang, and M. Chopp, "Intact, injured, necrotic and apoptotic cells after focal cerebral ischemia in the rat," *J. Neurol. Sci.* **156**(2), 119–132 (1998).
17. J. Xu, D. Kang, Y. Zeng, S. Zhuo, X. Zhu, L. Jiang, J. Chen, and J. Lin, "Multiphoton microscopy for label-free identification of intramural metastasis in human esophageal squamous cell carcinoma," *Biomed. Opt. Express* **8**(7), 3360–3368 (2017).
18. J. Chen, J. Xu, D. Kang, M. Xu, S. Zhuo, X. Zhu, and X. Jiang, "Multiphoton microscopic imaging of histological sections without hematoxylin and eosin staining differentiates carcinoma in situ lesion from normal oesophagus," *Appl. Phys. Lett.* **103**(18), 183701 (2013).
19. W. R. Zipfel, R. M. Williams, R. Christie, A. Y. Nikitin, B. T. Hyman, and W. W. Webb, "Live tissue intrinsic emission microscopy using multiphoton-excited native fluorescence and second harmonic generation," *Proc. Natl. Acad. Sci. U.S.A.* **100**(12), 7075–7080 (2003).
20. S. Bok, T. Wang, C. J. Lee, S. U. Jeon, Y. E. Kim, J. Kim, B. J. Hong, C. J. Yoon, S. Kim, S. H. Lee, H. J. Kim, I. H. Kim, K. H. Kim, and G. O. Ahn, "In vivo imaging of activated microglia in a mouse model of focal cerebral ischemia by two-photon microscopy," *Biomed. Opt. Express* **6**(9), 3303–3312 (2015).
21. X. Zhu, Y. Tang, J. Chen, S. Xiong, S. Zhuo, and J. Chen, "Monitoring wound healing of elastic cartilage using multiphoton microscopy," *Osteoarthritis Cartilage* **21**(11), 1799–1806 (2013).
22. D. A. Dombeck, K. A. Kasichke, H. D. Vishwasrao, M. Ingelsson, B. T. Hyman, and W. W. Webb, "Uniform polarity microtubule assemblies imaged in native brain tissue by second-harmonic generation microscopy," *Proc. Natl. Acad. Sci. U.S.A.* **100**(12), 7081–7086 (2003).
23. S. Wang, X. Chen, W. Wu, Z. Chen, H. Du, X. Wang, Y. V. Fu, L. Hu, and J. Chen, "Rapid, label-free identification of cerebellar structures using multiphoton microscopy," *J. Biophotonics* **10**(12), 1617–1626 (2017).
24. E. Z. Longa, P. R. Weinstein, S. Carlson, and R. Cummins, "Reversible middle cerebral artery occlusion without craniectomy in rats," *Stroke* **20**(1), 84–91 (1989).
25. M. Cai, Z. Yu, L. Wang, X. Song, J. Zhang, Z. Zhang, W. Zhang, W. Li, J. Xiang, and D. Cai, "Tongxinluo reduces brain edema and inhibits post-ischemic inflammation after middle cerebral artery occlusion in rats," *J. Ethnopharmacol.* **181**, 136–145 (2016).
26. T. H. Chia, A. Williamson, D. D. Spencer, and M. J. Levene, "Multiphoton fluorescence lifetime imaging of intrinsic fluorescence in human and rat brain tissue reveals spatially distinct NADH binding," *Opt. Express* **16**(6), 4237–4249 (2008).
27. O. Uckermann, R. Galli, S. Leupold, R. Coras, M. Meinhardt, S. Hallmeyer-Elgner, T. Mayer, A. Storch, G. Schackert, E. Koch, I. Blümcke, G. Steiner, and M. Kirsch, "Label-free multiphoton microscopy reveals altered tissue architecture in hippocampal sclerosis," *Epilepsia* **58**(1), e1–e5 (2017).
28. M. Tsacopoulos and P. J. Magistretti, "Metabolic coupling between glia and neurons," *J. Neurosci.* **16**(3), 877–885 (1996).
29. H. Du, L. Jiang, X. Wang, G. Liu, S. Wang, L. Zheng, L. Li, S. Zhuo, X. Zhu, and J. Chen, "Label-free distinguishing between neurons and glial cells based on two-photon excited fluorescence signal of neuron perinuclear granules," *Laser Phys. Lett.* **13**(8), 085603 (2016).
30. A. Coimbra, "Nerve cell changes in the experimental occlusion of the middle cerebral artery," *Acta Neuropathol.* **3**(6), 547–557 (1964).

31. D. Aggoun-Zouaoui, I. Margalli, F. Borrega, A. Represa, M. Plotkine, Y. Ben-Ari, and C. Charriaut-Marlangue, "Ultrastructural morphology of neuronal death following reversible focal ischemia in the rat," *Apoptosis* **3**(2), 133–141 (1998).
32. B. Chance and B. Schoener, "A correlation of absorption and fluorescence changes in ischemia of rat liver in vivo," *Biochem. Z.* **341**(4), 340 (1965).
33. M. A. Yaseen, S. Sakadžić, W. Wu, W. Becker, K. A. Kasischke, and D. A. Boas, "In vivo imaging of cerebral energy metabolism with two-photon fluorescence lifetime microscopy of NADH," *Biomed. Opt. Express* **4**(2), 307–321 (2013).
34. Q. Liu, J. Chen, S. Zhuo, X. Jiang, and K. Lu, "Nonlinear spectral imaging microscopy of rabbit aortic wall," *Chin. Opt. Lett.* **7**(3), 240–243 (2009).
35. S. W. Hou, Y. Q. Wang, M. Xu, D. H. Shen, J. J. Wang, F. Huang, Z. Yu, and F. Y. Sun, "Functional integration of newly generated neurons into striatum after cerebral ischemia in the adult rat brain," *Stroke* **39**(10), 2837–2844 (2008).
36. E. Candelario-Jalil, "Injury and repair mechanisms in ischemic stroke: considerations for the development of novel neurotherapeutics," *Curr. Opin. Investig. Drugs* **10**(7), 644–654 (2009).
37. U. Dirnagl, C. Iadecola, and M. A. Moskowitz, "Pathobiology of ischaemic stroke: an integrated view," *Trends Neurosci.* **22**(9), 391–397 (1999).
38. A. Arvidsson, T. Collin, D. Kirik, Z. Kokaia, and O. Lindvall, "Neuronal replacement from endogenous precursors in the adult brain after stroke," *Nat. Med.* **8**(9), 963–970 (2002).
39. S. Fumagalli, J. A. Coles, P. Ejlerskov, F. Ortolano, T. J. Bushell, J. M. Brewer, M. G. De Simoni, G. Dever, P. Garside, P. Maffia, and H. V. Carswell, "In vivo real-time multiphoton imaging of T lymphocytes in the mouse brain after experimental stroke," *Stroke* **42**(5), 1429–1436 (2011).
40. S. Psilodimitrakopoulos, V. Petegnief, N. de Vera, O. Hernandez, D. Artigas, A. M. Planas, and P. Loza-Alvarez, "Quantitative imaging of microtubule alteration as an early marker of axonal degeneration after ischemia in neurons," *Biophys. J.* **104**(5), 968–975 (2013).
41. C. J. Schrandt, S. M. S. Kazmi, T. A. Jones, and A. K. Dunn, "Chronic monitoring of vascular progression after ischemic stroke using multiexposure speckle imaging and two-photon fluorescence microscopy," *J. Cereb. Blood Flow Metab.* **35**(6), 933–942 (2015).
42. W. Piyawattanametha, E. D. Cocker, L. D. Burns, R. P. Barretto, J. C. Jung, H. Ra, O. Solgaard, and M. J. Schnitzer, "In vivo brain imaging using a portable 2.9 g two-photon microscope based on a microelectromechanical systems scanning mirror," *Opt. Lett.* **34**(15), 2309–2311 (2009).
43. F. Helmchen, W. Denk, and J. N. D. Kerr, "Miniaturization of two-photon microscopy for imaging in freely moving animals," *Cold Spring Harb Protoc.* **2013**(10), pdb.top078147 (2013).

1. Introduction

Stroke is a leading cause of death and permanent disability worldwide, in which ischemic injury results from vascular occlusion and a subsequent cerebral infarction [1, 2]. Interrupted blood supply to the brain causes abrupt oxygen and nutrient deprivation and results in typical pathophysiological events that temporally and spatially evolve. Neurons die primarily by necrosis acutely after insult. Subsequently, tissue damage expands from the core into surrounding healthy tissue of the penumbra and this subacute phase lasts approximately six to twenty-four hours. Finally, secondary phenomena including vasogenic edema and inflammation develop during a delayed injury phase that lasts for days to weeks after insult [3, 4]. Middle cerebral artery occlusion (MCAO) in rats is a simple and widely accepted animal model for studies of cerebral ischemic pathophysiology and therapeutic interventions [5–7]. The degree and extent of cerebral tissue injury is directly related to the duration of MCAO. Necrotic death mainly affects cells in the ischemic core and delayed death impacts susceptible neurons in neighboring regions. As cell death in injury core-adjacent regions occurs over an extended period of time, these neurons may be targeted for rescue by pharmacological agents and other therapies. The temporal and spatial progression of ischemic cell damage and its dependence on blood flow suggest that modulators of blood vessel integrity affect the magnitude of damaged tissue and the speed at which damage occurs [8]. Therefore, spatial and temporal identification of the boundaries of the infarct core as well as the discrimination of differentially affected perilesional areas is essential to investigate correlations between the extent of neuroprotection or the variability of post-ischemic gene regulation with a defined degree of injury [9–11].

With advancements in characterizing biological features of ischemic stroke and improved diagnostic techniques, non-invasive methods such as magnetic resonance imaging (MRI), perfusion computerized tomography (CT), and positron emission tomography (PET) that not

only provide anatomical, physiological, and molecular information, but also obtain inherently quantifiable information in widespread clinical use [12–14]. For suspected acute stroke or transient ischemic attack, a brain CT or MRI scan is urgently recommended for all patients [15]. However, some disadvantages and limitations in these imaging technologies remain, including low resolution, poor contrast sensitivity, and necessity for contrast medium. Although an increasing variety of fluorescent dyes and gene techniques have been implemented to address these issues, they also have unavoidable shortcomings related to increased time consumption for application and associated cellular damage [10, 16]. Therefore, the development of label-free and noninvasive methods is needed for better identifying the ischemic infarct core in time and space.

Recently, multiphoton microscopy (MPM) based on two-photon excited fluorescence (TPEF) and second harmonic generation (SHG) have demonstrated the potential for noninvasive visualization of tissue architecture at the cellular level [17, 18]. Such methods have exhibited the ability to detect biological tissues and changes in these tissues with high resolution and high sensitivity. According to previous research, abundant intrinsic fluorophores are present in biological tissues emitting high TPEF signals, such as nicotinamide adenine dinucleotide (NADH), nicotinamide adenine dinucleotide phosphate (NADPH), flavin adenine dinucleotide (FAD), retinol, and tryptophan and its indoleamine derivatives [19–21]. These distinctions are not clearly revealed by traditional histopathology. In addition, axon fibers with non-centrosymmetric molecular structure are most effective in producing SHG signals [22, 23]. Therefore, MPM has become an attractive tool for identifying the infarct core as well as the different perilesional areas following cerebral ischemia.

In the present study, we investigated whether MPM based on label-free SHG and intrinsic TPEF of intracellular sources can identify normal and ischemic brain tissue. We then characterized a detailed time-course of neurodegeneration following different time periods of MCAO. Our characterization included both the cortex and the striatum region based on both TPEF and SHG signals, in which neurons undergo morphological changes. The findings of this study will hopefully promote awareness and advancement of the use of noninvasive modalities to discriminately characterize injured and spared brain tissue following ischemic events.

2. Materials and methods

2.1 Sample preparation

In this study, we selected the reliable and less invasive rat MCAO stroke model to obtain and evaluate the extensive morphological neural data. All animal experiments were approved by the Institutional Animal Care and Use Committee of Fujian Medical University and were performed in accordance with the National Institute of Health Guide for the Care and Use of Laboratory Animals. Male Sprague-Dawley (SD) rats (6–8 weeks) weighing 250–300 g were provided by Shanghai Laboratory Animal Co., Ltd., China (license no. SCXK 2014-007) for this study and MCAO was performed as previously described [24]. In brief, rats were anesthetized with an intravenous injection of 2.5% sodium pentobarbital (2 ml/kg), and the left middle cerebral artery was permanently occluded using a commercial monofilament nylon suture. During surgery, the animal's body temperature was maintained at 37°C using a heating pad. After suturing and closing the surgical site, the rats were placed in a cage under an infrared heating lamp until recovery from anesthesia. The surviving rats were euthanized by decapitation and the brain was removed at various times after the onset of occlusion (6, 24, 48, and 72 hours; $n = 6$ each). The whole brain was removed after onset of occlusion and segmented into five parts from the anterior to posterior region in the coronal plane to measure the infarct area. Then each part was cut into three consecutive coronal sections of 10 μm thickness with a freezing microtome. Since the sections are very thin, there are slight structural differences between the three sections. As illustrated in Fig. 1(A), the middle

section (black frame) was stained with hematoxylin-eosin (H&E) for histological analysis, and the adjacent two sections (blue frames) were used for MPM imaging. During the MPM experiment, a small volume of phosphate-buffered saline (PBS) solution was dripped onto the tissue specimen in order to avoid dehydration or shrinkage.

2.2 Imaging instrumentation

The multiphoton imaging system used in this study contained an inverted Axiovert 200 microscope (LSM 510 META; Carl Zeiss, Inc.) coupled to a mode-locked femtosecond Ti:sapphire laser (110 fs, 76 MHz) operating at 810 nm (Mira 900-F). The polarization of laser light was linear. For high-resolution imaging, an oil immersion objective (Plan-Apochromat 63 \times , NA = 1.4, Zeiss) was used for focusing the excitation beam into brain samples and backscattered intrinsic SHG and TPEF signals were collected. The excitation power was 5-10 mW on the specimen surface. For 810 nm, resolution of 0.3 μ m (lateral) and a 0.8 μ m (axial) can be expected. The signals were directed to the META detector by a main dichroic beam splitter (HFT KP650, Carl Zeiss, Inc.). Two different channels of the META detector were selected for obtaining high contrast images. One channel covered the 430 to 709 nm wavelength range to produce the tissue TPEF image (red color-coded). The other channel corresponded to the 388 to 419 nm wavelength range for SHG images (green color-coded). In our study, for 810 nm excitation, the second harmonic signal was a sharp peak at 405 nm. Specifically, the 475 nm peak and 535 nm peak respectively corresponded to the nicotinamide adenine dinucleotide (NADH), and flavin adenine dinucleotide (FAD) [34]. An optional HRZ 200 fine focusing stage (Carl Zeiss) was utilized to move the motorized x-y scanning stage to obtain large-area images and modify the focus position for recording various optical sections. All images had a 12-bit pixel depth and were acquired at a rate of 2.56 μ s per pixel.

In addition, the light microscope (Eclipse Ci-L, Nikon Instruments Inc., Japan) was used for imaging H&E stained sections equipped with a charge-coupled device (CCD) camera (Nikon, DS-Fi2, Japan).

2.3 Measurement of infarct area

For each brain, the five H&E stained sections were examined to calculate the infarct area. Firstly, each H&E stained section was imaged using a light microscope equipped with a CCD camera and the image was displayed on a computer screen. And then, a boundary between normal and infarct areas was drawn by using Image-Pro Plus 6.0 software, and the infarct area was automatically measured to calculate the percentage of the infarct area. Furthermore, the boundary between the infarct and normal areas was verified by a certified pathologist. Finally, the percentage of the infarct area was adjusted to avoid the edema-associated error according to the following formula: Corrected Infarct Area = [Contralateral Hemisphere Area – (Ipsilateral Hemisphere Area – Infarct Area)] / (2 \times Contralateral Hemisphere Area) \times 100% [25].

2.4 Quantification analysis

The neurons in the cortex and striatum have distinctive histological characteristics at various time-points after MCAO. To accurately distinguish between normal and ischemic brain tissue, two parameters including the ratio of injured to normal neurons and the nuclear-to-cytoplasmic ratio in injured or normal neurons were calculated. The ratio of injured to normal neurons was calculated by dividing the number of injured neurons by the number of normal neurons as determined through histologic observation. For nuclear-to-cytoplasmic ratio analysis, the area of the nucleus and cell was measured automatically by LSM 510 software. The nuclear-to-cytoplasmic ratio was calculated by dividing the nuclear area by the cytoplasmic area, and expressed by Nuclear-to-Cytoplasmic Ratio = Nuclear Area / (Cell Area - Nuclear Area). The final results were expressed as the mean value \pm standard deviation (mean \pm SD). Data groups were subjected to the Shapiro-Wilk test and followed a normal

distribution when $p > 0.05$. A two-tailed Student's t test was then performed to determine significant differences between any two groups. For comparison of multiple groups, one-way analysis of variance (ANOVA) was assessed using SPSS software (version 21.0, IBM, New York, USA). Differences were regarded as statistically significant when $p < 0.05$.

3. Results

3.1 General results

As illustrated in Fig. 1(A), the brain was segmented into five parts from the anterior to posterior region in the coronal plane and then each part was further cut into three consecutive coronal sections of 10 μm thickness. The middle section (black frame) was stained with H&E for a histological comparison with the results of MPM. Figure 1(B) presented the sequence of the five H&E stained coronal sections at 6 hours post-MCAO. Since the left middle cerebral artery of Sprague-Dawley (SD) rats was occluded, the acute necrosis occurred in left hemisphere that consistently included the cerebral cortex, corpus striatum, globus pallidus, amygdala, hippocampus, and much of the septum, thalamus and hypothalamus. It can be seen that the affected left hemisphere was lighter in color than normal regions at 6 hours post-MCAO. The boundary between the infarct and normal areas was marked with black solid lines by Image-Pro Plus 6.0 software. In examining all of the H&E stained sections, the core of the ischemic infarct was clearly detectable at all time-points investigated after permanent MCAO, and the infarct size depended on time of occlusion duration. As shown in Fig. 1(C), the measurement of the infarct areas showed significantly increased infarct size with longer occlusion duration. Specifically, the percentage of infarct area was $24.65 \pm 2.27\%$ ($n = 6$) at 6 hours post-MCAO, $30.27 \pm 3.69\%$ ($n = 6$) at 24 hours, $32.12 \pm 4.60\%$ ($n = 6$) at 48 hours, and $39.99 \pm 3.65\%$ ($n = 6$) at 72 hours.

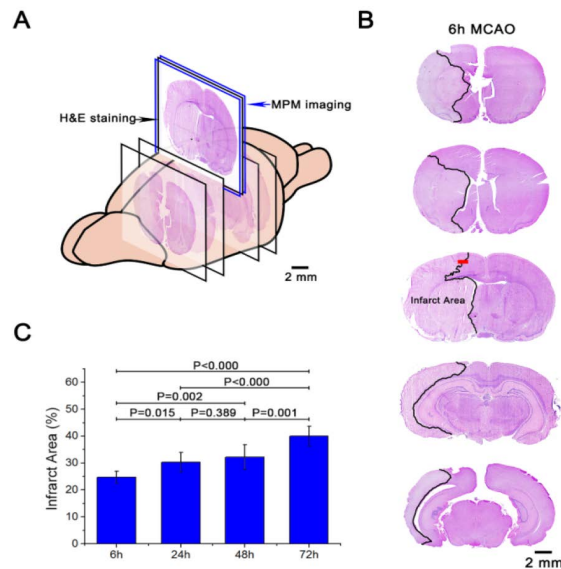


Fig. 1. (A) The diagram of sample preparation. (B) The sequence of the five H&E stained coronal sections ($4 \times$ magnification) at 6 hours after permanent MCAO. The boundary between infarction and normal brain was marked with a black solid line. (C) The percentage of infarct area at various times shows significantly increased infarction with increasing occlusion duration.

3.2 Identification of ischemic regions

Focal cerebral ischemia results in cell injury and death at the lesion core and ischemic penumbra. Identification of the ischemic regions will allow for improved understanding of the spatial progression of ischemic cell damage and to better correlate the extent of therapy-mediated neuroprotection.

As presented in Fig. 2(A), a representative TPEF image of normal cerebral cortex showed numerous neuron and glial cells in the cortex. Moreover, the magnified frame (inset) clearly depicted more detailed information of individual neuron and glial cell. As we can see from the figure, cytoplasmic NAD(P)H and FAD emitted strong TPEF signals while non-fluorescent cell nuclei appeared as dark spots, which highlighted the distinguishable individual cells. Some cell nuclei were visibly surrounded by a large number of cytoplasmic granules emitting high TPEF signals (white arrowheads). According to the previous study, cells that exhibited extensive cytoplasmic granules were neurons (white arrowheads) [26, 27], the bright punctate granules were NADH-rich mitochondria [28], while the cells with few or without granules were glial cells (arrows) [29]. These observations indicated a distinct photochemical composition of the cytoplasmic content in neurons compared to glial cells. By contrast, TPEF images of cortex from an infarct core after 6 hours of permanent MCAO were shown in Fig. 2(B). According to the previous study, a well-defined line of separation between healthy neurons and injured neurons was the exhibition of either intense pathological shrinkage or extensive cytoplasmic vacuolization as in the hydropic change [30]. In Fig. 2(B), we can see numerous injured neurons were located in ischemic infarct core. Each injured neuron exhibited condensed morphology, a contracted nucleus and brightened cytoplasm (yellow arrowheads). In addition, all normal cell nuclei lacked fluorescent signals and appeared as dark round shapes, while the nuclei of injured neurons were irregular in appearance, and injured neurons assumed a triangular shape that distinguished it from a normal healthy neuron. However, a few surviving neurons were seen in the infarct area (white arrowheads). The different features of neurons in normal and injured cortex were consistent with corresponding H&E staining, as illustrated in Figs. 2(D) and 2(E), respectively. Clear nuclear shrinkage of injured neurons was evident based on blue hematoxylin stain. Necrotic neurons showed extreme shrinkage with widened pericellular spaces, nuclear pyknosis and cytoplasmic eosinophilia, followed by fading [31]. Quantitatively, the nuclear-to-cytoplasmic ratios of normal and injured neurons after 6 hours of MCAO were 0.51 ± 0.12 ($n = 20$) and 0.27 ± 0.07 ($n = 20$), respectively ($p < 0.001$, two-tailed Student's *t* test). Moreover, the average area of neuronal nuclei was also measured, which were 53.45 ± 13.72 ($n = 20$) and 36.64 ± 2.77 ($n = 20$) of normal and injured neurons after 6 hours of MCAO, respectively ($p < 0.001$, two-tailed Student's *t* test). These results clearly indicated significantly reduced nuclear-to-cytoplasmic ratio and average area of neuronal nuclei of injured neurons compared to normal neurons, and this finding quantitatively reflected nuclear shrinkage in injured neurons.

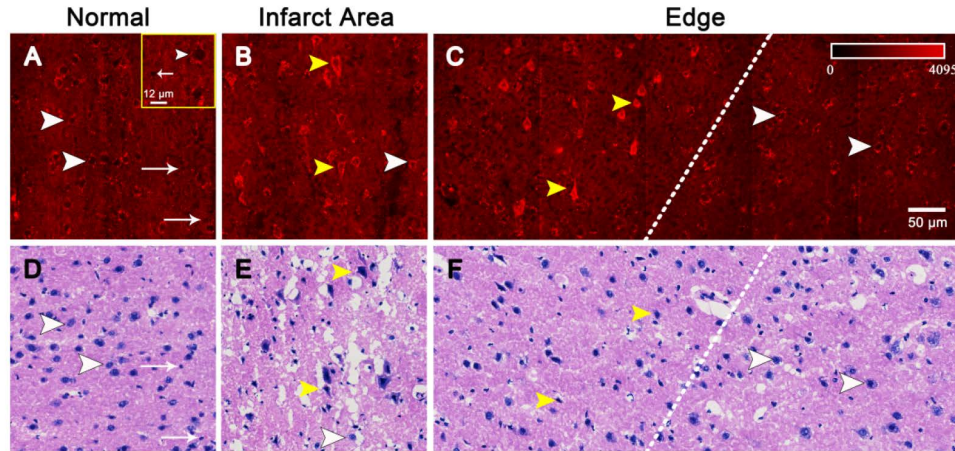


Fig. 2. TPEF images of cerebral cortex from (A) a normal brain section, (B) an infarct core, and (C) a partial edge of the infarction. The color bar indicates the minimum and maximum signal intensities. The corresponding H&E stained images of cerebral cortex from (D) a normal brain section, (E) the infarct core, and (F) the partial edge of the infarction. Inset frame in (A): representative neurons and glial cells. Normal neurons: white arrowheads; injured neurons: yellow arrowheads; glial cells: arrows; white dashed lines: the boundary between normal and infarct area. The color bar indicates the range of TPEF intensity.

Figure 2(C) represented a large-area TPEF image of the partial edge of the infarct area after 6 hours of permanent MCAO (red squared area in Fig. 1(B)). This region exhibited differences in cellular morphology and TPEF intensity of neuronal cytoplasm between the normal (right side) and infarct areas (left side). The color bar indicated the range of TPEF intensity. In particular, Fig. 2(C) had slight black vertical lines which produced by the automated mosaic process. Additionally, since the sections were very thin, the arrows in the MPM image and H&E stained image had slight position errors. In the normal area, granular substance surrounded neuronal nuclei (white arrowheads) and these neurons presented with a typically salient round cell body. However, triangular-shaped injured neurons (yellow arrowheads) were distributed in the infarct area. Quantitatively, TPEF intensity of neuronal cytoplasm showed significant differences between normal and injured neuron after 6 hours of MCAO were 1461.45 ± 227.69 ($n = 20$) and 2289.80 ± 211.42 ($n = 20$), respectively ($p < 0.001$, two-tailed Student's *t* test). According to previous research, ischemic hypoxia caused acute interruption of oxidative phosphorylation in cellular respiratory chain, which was associated with prompt increase in NADH levels [32]. And all observable NADH species increased sharply during the onset of occlusion [33]. Therefore, TPEF signal from the pericellular substances of injured neurons was stronger than that of normal neurons, which was due to the increased NAD(P)H fluorescence. In the corresponding H&E stained image (Fig. 2(F)), injured (yellow arrowheads) and normal neurons (white arrowheads) were only identified based on the cellular shapes. The boundaries were drawn in Fig. 2(C) and (F), which were confirmed by a certified pathologist. These results demonstrated that TPEF microscopy cannot only obtain distinctly neuronal morphologic characteristics for identifying normal and injured neurons, but also provide quantitative assessment of condensed neuronal morphology and increased TPEF intensity of neuronal cytoplasm between normal and infarct regions, which had greater potential to identify ischemic regions compared to traditional pathological analysis.

3.3 Cortical neuron morphology varied with duration of occlusion

The duration of MCAO was known to be a primary determinant of the degree of injury severity and highly influences the outcome following this surgery. Figure 3 showed TPEF

images and corresponding H&E stained images of the ischemic cortex from the ischemic core at 6, 24, 48, and 72 hours after MCAO. The injured neurons exhibited shrunken morphology with widened pericellular spaces and nuclear pyknosis, and varied in extent and severity with the duration of MCAO.

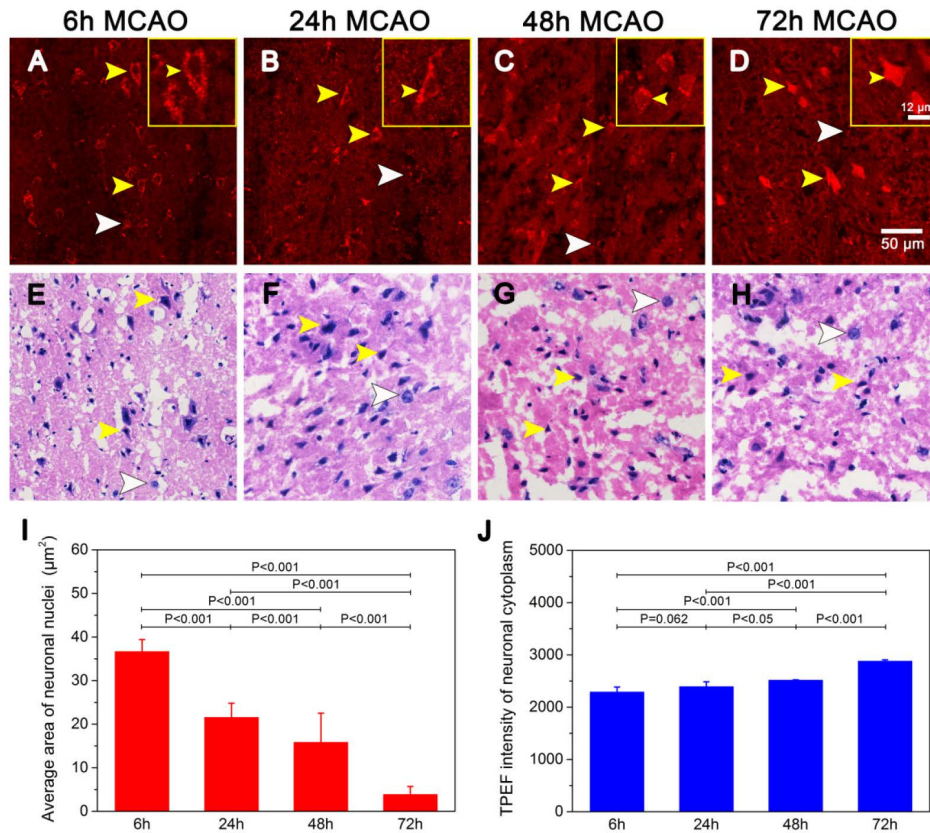


Fig. 3. TPEF (A-D) and corresponding H&E stained images (E-H) of neuronal necrosis in the cerebral cortex varied with occlusion duration of 6, 24, 48, and 72 hours after MCAO. (I) Average area of neuronal nuclei. (J) TPEF intensity of neuronal cytoplasm. Inset frames: representative magnified injured neurons; Normal neurons: white arrowheads; injured neurons: yellow arrowheads.

At 6 hours post-MCAO, injured neurons exhibited an irregular shape and nuclear pyknosis observed as non-fluorescent spots and increased pericellular substance emitting strong TPEF signals (yellow arrowheads). There were still a few surviving neurons found in the damaged tissue region (white arrowheads). At 24 hours post-MCAO, pericellular substances with much stronger TPEF signals were observed surrounding shrunken non-fluorescent nuclei. Since ischemic hypoxia results in increased in NADH levels [32], the stronger TPEF signals at 24 hours post-MCAO indicated more severe injury of neurons. Furthermore, non-fluorescent nuclei were hardly observed at 48 and 72 hours after MCAO. Numerous necrotic neurons were evident by strong TPEF signals from pericellular substance, and focal necrosis was sometimes observed. Moreover, few normal neurons were observed at 24 hours post-MCAO and almost none after 72 hours. We then measured the average area of neuronal nuclei as well as TPEF intensity of neuronal cytoplasm from the ischemic cortex with occlusion duration of 6, 24, 48, and 72 hours after MCAO. For comparison, the average

area of neuronal nuclei had reduced significantly, which was 36.64 ± 2.77 ($n = 20$) at 6 hours, 21.52 ± 3.29 ($n = 20$) at 24 hours, 15.82 ± 6.69 ($n = 20$) at 48 hours, and 3.87 ± 1.87 ($n = 20$) at 72 hours (Fig. 3(I)). However, an overall progressive increased in TPEF intensity of neuronal cytoplasm was observed (Fig. 3(J)). The intensity was 2289.8 ± 211.45 ($n = 20$) at 6 hours, 2391.35 ± 95.46 ($n = 20$) at 24 hours, 2516.65 ± 7.78 ($n = 20$) at 48 hours, and 2880.55 ± 511.95 ($n = 20$) at 72 hours following MCAO, respectively. The severity of neuronal injury and occlusion duration were directly related. These results demonstrated that TPEF microscopy can also be used to evaluate the structural changes of injured neurons at various ischemic time-points, which were essential to understanding the basic pathophysiology of cerebrovascular ischemia, as well as to evaluating the effect of treatment regimens.

3.4 Structural alterations in the striatum

Ischemic injury to the striatum was examined in addition to the cerebral cortex. This region was of particular interest because it consisted of an intimate mixture of neurons and axon fiber bundles. The emission spectrum of striatum as well as cortex at an excitation wavelength of 810 nm was shown in Fig. 4. It was evident that TPEF (430-716 nm) and SHG (peak at 405 nm) signal were completely separated. According to our previous studies, the 475 nm peak and 535 nm peak respectively corresponded to the NADH and FAD fluorescence for 810 nm excitation [34]. The 405 nm peak of axon bundles resulted from microtubule arrays with uniform polarity inside myelinated axons comprised of tubulin with hyperpolarizability and asymmetric structures along its longitudinal axis [22]. Moreover, the obvious difference in the emission spectrum at 405 nm indicated that MPM could be used for spectral discrimination between the striatum and cortex.

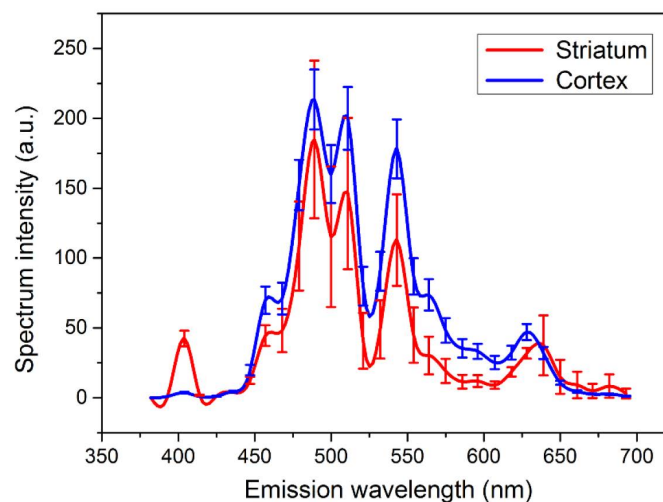


Fig. 4. The emission spectrum of cortex and striatum at an excitation wavelength of 810 nm.

Representative individual TPEF and SHG images, their overlaid images, and corresponding H&E stained images of normal and ischemic striatum were presented from coronal sections of the rat brain at various times after MCAO (Fig. 5). TPEF signals (red color coded, Figs. 5(A)-5(E)) from NAD(P)H and FAD in the cytoplasm highlighted distinguishable individual cells (white arrowheads). In addition, axon bundles also produced TPEF signals (red color-coded, asterisks in Figs. 5(A)-5(E)) even though they were the main source of SHG signals (green color-coded, asterisks in Figs. 5(F)-5(J)) in the striatum. The detailed structure of the striatum was depicted in the overlaid TPEF/SHG images (Figs. 5(K)-5(O)). In Fig. 5(K), individual neurons (white arrowheads) could be readily resolved between

axon bundles due to characteristic non-fluorescent nuclei surrounded by cytoplasm. Cytoplasmic granules of neurons and extracellular matrix emitted strong TPEF signals which were shown in red. However, axon bundles (asterisk) ran perpendicular to the image plane and emitted comparable SHG (green color coded) and TPEF (red color coded) signals at the same order of magnitude, which presented as a yellow color. Consequently, dense cellular regions appeared red whereas tightly packed axon bundles appeared yellow.

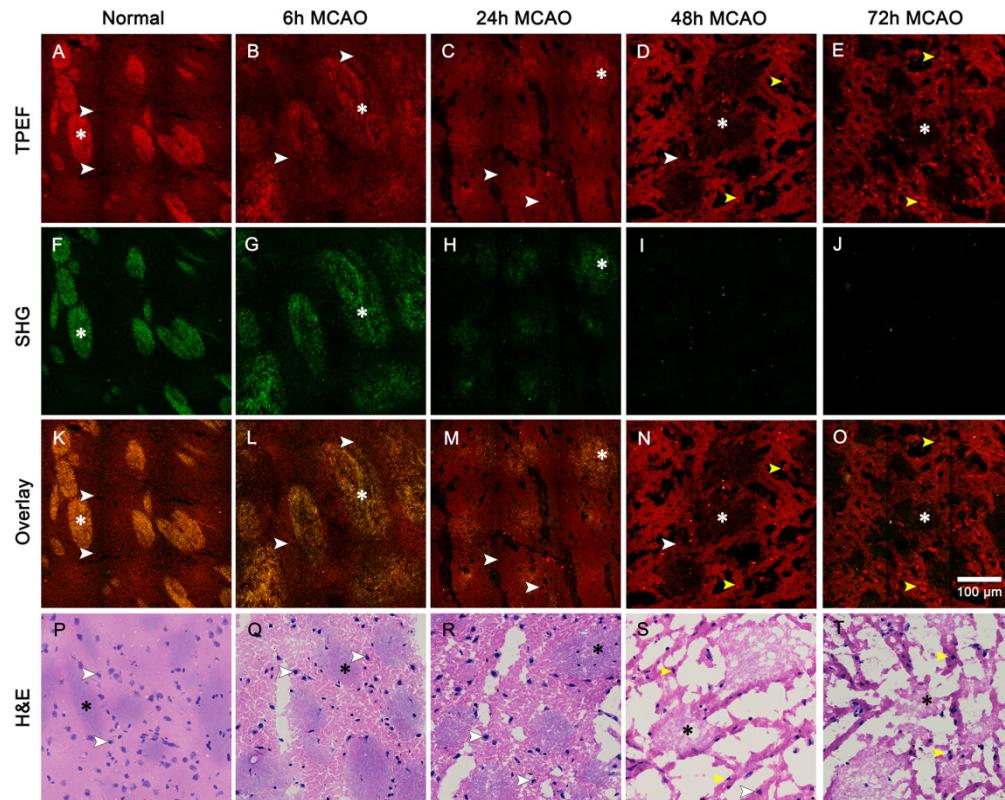


Fig. 5. TPEF, SHG, their overlaid images, and corresponding H&E stained images of striatum sectioned in the coronal plane of normal and ischemic rat brain at 6, 24, 48, and 72 hours after MCAO. (A-E): TPEF image (red); (F-J): SHG image (green); (K-L): overlaid images; (P-T): corresponding H&E stained images. Axon bundles: asterisk; neurons: white arrowheads; injured neurons: yellow arrowheads.

Furthermore, lesions varied in injury severity of neurons and axon bundles with occlusion time. Comparison of TPEF images (Figs. 5(A)-5(E)) showed that the histologic alterations of neurons in the striatum resembled those described in the cortex. However, delayed damage and degeneration was demonstrated in the striatum compared to the cortex. In addition, axon fiber damage in the striatum was observed at various times after MCAO (Figs. 5(F)-5(J)). Signals from axon bundles weakened gradually with increased occlusion time. At 6 hours post-MCAO (Fig. 5G), axon bundles in more severe lesions were pale and swollen. At 24 hours post-MCAO, partly necrotic areas showed loss of myelinated fibers (Fig. 5(H)). Completely necrotic areas showed even greater loss of myelinated fibers at 48 and 72 hours after MCAO (Figs. 5(I) and 5(J)). In the most severe lesions, the tissue architecture was completely destroyed, leaving fragmented and granular eosinophilic debris, or a loose meshwork of fibers, traversed by persisting capillaries and phagocytes [35]. Comparison of the overlaid TPEF/SHG images also revealed structural alterations of axon bundles with the duration of occlusion (Figs. 5(K)-5(O)). Compared to the corresponding H&E stained images

(Figs. 5(P)-5(T)), our results indicated that composite TPEF and SHG microscopy was capable of generating comparable images of microscopic architecture of striatum at various times after MCAO.

3.5 Quantification of injured neurons

To further quantitatively describe neuronal injury severity in cortical and striatal brain regions, the ratio of injured over normal neurons and the nuclear-to-cytoplasmic ratio of normal and injured neurons were calculated. Quantitative analysis revealed a significant association between the nuclear-to-cytoplasmic ratio and the injury severity of MCAO. For comparison, the cortical neuron nuclear-to-cytoplasmic ratio was 0.27 ± 0.07 ($n = 20$) at 6 hours, 0.16 ± 0.04 ($n = 20$) at 24 hours, 0.14 ± 0.05 ($n = 20$) at 48 hours, and significantly reduced to 0.04 ± 0.06 ($n = 20$) at 72 hours, as shown in Fig. 6(A). Similar to this trend, quantification showed that the nuclear-to-cytoplasmic ratio of striatum neurons was 0.45 ± 0.12 ($n = 20$) at 6 hours, 0.46 ± 0.11 ($n = 20$) at 24 hours, 0.27 ± 0.08 ($n = 20$) at 48 hours, and 0.05 ± 0.05 ($n = 20$) at 72 hours, as also exhibited in Fig. 6(B). From these observations, the evidence suggested that the nuclear-to-cytoplasmic ratio significantly decreased with the development of nuclear pyknosis or cytoplasmic edema.

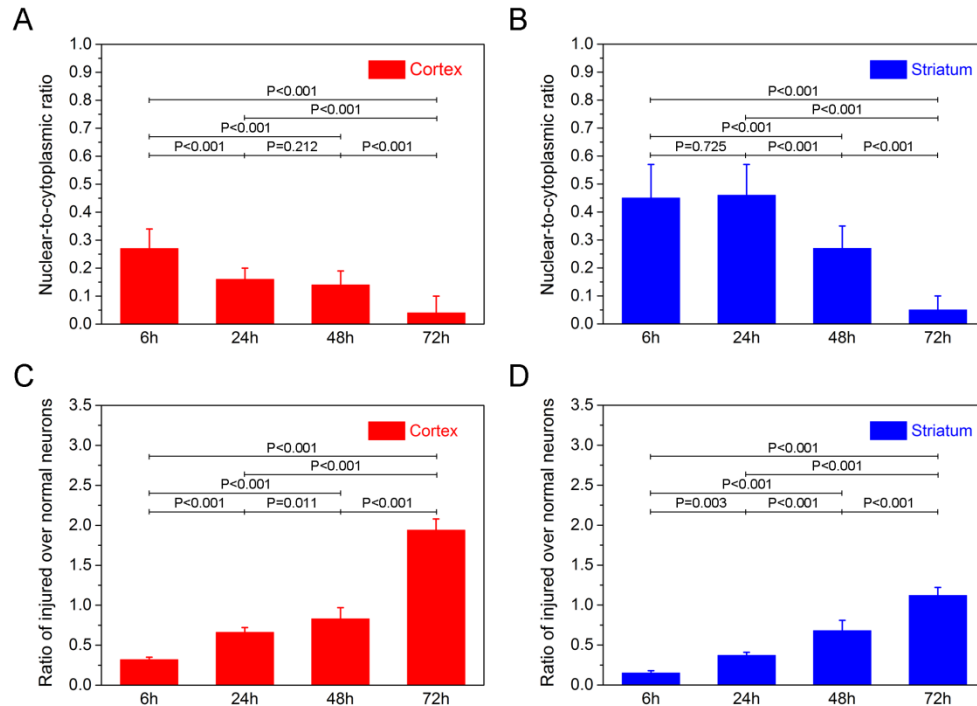


Fig. 6. The nuclear-to-cytoplasmic ratio of neurons in cortex (A) and striatum (B) varied with occlusion duration. The ratio of injured neurons over normal neurons in cortex (C) and striatum (D) varied with occlusion duration.

In addition, variable duration of permanent MCAO caused neuronal degradation; therefore, the ratio of injured to normal neurons in the cortex and striatum may be used to differentiate the extent of ischemic injury. Our measurements showed that the ratio of injured over normal neurons in cortex was 0.32 ± 0.03 ($n = 20$) at 6 hours, 0.66 ± 0.06 ($n = 20$) at 24 hours, 0.83 ± 0.14 ($n = 20$) at 48 hours, and 1.94 ± 0.14 ($n = 20$) at 72 hours post-MCAO (Fig. 6(C)). However, the ratio of injured over normal neurons in striatum had different results. This ratio was 0.15 ± 0.03 ($n = 20$) at 6 hours, 0.37 ± 0.04 ($n = 20$) at 24 hours, 0.68 ± 0.13 ($n = 20$) at 48 hours, and 1.12 ± 0.10 ($n = 20$) at 72 hours following MCAO, respectively

(Fig. 6(D)). These findings clearly indicate that number of normal healthy neurons was significantly reduced with increased time following permanent MCAO (Fig. 6(C) and (D)). In general, the lesions showed a complete spectrum of gradations in severity and size based on the duration of occlusion.

4. Discussion

Ischemic stroke triggers a complex and highly interconnected cascade of cellular and molecular changes. The changes induced following ischemic injury, including calcium overload, oxidative stress neuroinflammation and cell death [36]. MPM, based on the advancement of the field of nonlinear optics and femtosecond lasers, can reveal details of the brain at the cellular and molecular level using a combination of autofluorescence from cells and SHG signal from collagen and microtubules. In this study, MPM was employed to visualize the cortex and striatum, which are susceptible to ischemic injury. This technique delivered high-resolution images of these two regions that afforded detailed information for assessing neuron and axonal changes at different durations of MCAO. Furthermore, spatial and temporal identification of the infarct core and perilesional areas were achieved. Compared to classic H&E staining, MPM was more effective in distinguishing normal from injured neurons. In general, H&E stained histopathology is a gold standard for diagnosing disease. However, the H&E histopathologic staining procedure has some disadvantages. For example, considerable time is required for staining steps and it is not suitable for real-time imaging. By contrast, MPM affords real-time imaging of ischemic tissues without destructive procedures and staining. In addition, all images had a 12-bit pixel depth and were acquired at a rate of 2.56 μ s per pixel. Therefore, multichannel detection, combined with increased accuracy and speed, makes MPM highly suitable for characterizing temporal morphologic features of neurons and axon bundles at subcellular resolution following MCAO compared to H&E staining.

Studies concerning potential protective strategies for ischemic stroke have typically focused on the neuron [37], as neurons are highly susceptible to injury and death after stroke. As injury and loss of neurons leads to various cognitive and sensorimotor dysfunctions, it is reasonable that targeting neurons for such therapies is a priority in stroke research. In the present study, MPM permitted visualization of injured neuronal features at 6, 24, 48, and 72 hours after MCAO, including contracted nuclei, condensed cytoplasmic shape, and brightened cytoplasmic signal intensity. Moreover, neuronal features were quantified from TPEF images, showing significant differences in the average area of neuronal nuclei, TPEF intensity of neuronal cytoplasm, as well as neuronal nuclear-to-cytoplasmic ratio, injured over normal neurons ratio at various times after MCAO. Quantitative assessment of changes in neuronal morphology will provide a useful reference for better understanding of injury progression in ischemic stroke. As such, the average area of neuronal nuclei, TPEF intensity of neuronal cytoplasm, as well as nuclear-to-cytoplasmic ratio may serve as a potential indicator for the extent of neuronal injury. And the ratio of injured over normal neurons will likely be more useful and intuitive for determining the degree of severity of ischemic injury.

Current high-resolution observation at the cellular and molecular level following ischemic stroke is typically accomplished using fluorescent-based microscopy techniques [21, 38]. However, these techniques require exogenous fluorescence markers to produce the necessary labeling and contrast. A key advantage of MPM is that it does not require the use of such external markers, which has permitted the study of various functional aspects of the brain at the cellular and molecular level including the structural dynamics of microtubule and cortical vasculature after ischemia [38–41]. Despite the power and extent of information that MPM can provide, some limitations still exist for applying MPM imaging to cerebral ischemia in the clinic, especially in imaging depth and miniaturization. Such visualization requires an appropriate application for in vivo monitoring combined with invasive optical fiber penetration of brain tissue. Fortunately, advances in the development of two-photon

fiberscopes and microendoscopic imaging devices offer new possibilities for performing deep in vivo brain imaging [42, 43]. The study presented here provides the groundwork for furthering the clinical imaging capabilities in ischemic stroke cases. The benefits of MPM make it possible to directly acquire high resolution histological diagnostic imaging in a clinical setting. In addition, this system is advantageous for developing and screening therapeutic agents for ischemic stroke.

In conclusion, MPM was employed to spatially and temporally identify cerebral infarction following MCAO. High resolution and high contrast images revealed detailed microstructures of normal brain tissue versus ischemic regions, and the boundaries separating the two were easily identified based on the morphological differences between healthy and injured neurons in ischemic tissue. In addition, the influence of occlusion duration on neuronal morphology variation was examined in the cerebral cortex and striatum. Based on TPEF signals and quantification, the ratio of injured to normal neurons increased with prolonged occlusion duration in both cortical and striatum regions. These findings are consistent with our understanding that neuronal necrosis is more extensive with increased duration of occlusion. In addition, the neuronal nuclear-to-cytoplasmic ratio decreased as occlusion period increased in the cerebral cortex and striatum. This corresponds to and supports previous results showing that nuclei shrink with increasing occlusion time and injury severity.

Taken together, the results of this study support the use of MPM as the method of choice for studying ischemic injury and its impact on neurons and axon fibers in the brain. Our findings demonstrated that MPM is effective in the spatiotemporal identification of ischemic regions in a rat model of MCAO by observing the TPEF signal from neurons and SHG from fibers. A recent study accomplished in vivo imaging of cerebral ischemia by looking at activated cells using intravenous fluorescent antibody injection in wild type animals [20]. Combining this advanced technology with the development of miniaturized MPM devices, MPM may be a powerful tool for diagnostic screening and monitoring cerebral ischemia.

Funding

National High Technology Research and Development Program of China (2015AA020508); the Joint Funds of Fujian Provincial Health and Education Research (WKJ2016-2-28); the National Natural Science Foundation of China (Grant No. 81671730); the National Key Basic Research Program of China (2015CB352006); the Program for Changjiang Scholars and Innovative Research Team in University (Grant No. IRT_15R10); and the Natural Science Foundation of Fujian Province (2015J01241, 2018J07004).

Acknowledgments

We would like to thank Xiaoting Zheng and Qingshuang Li in Fujian Medical University, for guidance in establishing the MCAO rat stroke model used in the study.

Disclosures

The authors declare that there are no conflicts of interest related to this article.